

# Optimal Design of SMB Units: A Novel Strategy Based on Particles Swarm Optimization

Joana Matos, Rui P.V. Faria, José M. Loureiro, Ana M. Ribeiro, Idelfonso B. R. Nogueira\*

\* *Laboratory of Separation and Reaction Engineering, Associate Laboratory LSRE-LCM  
Department of Chemical Engineering, Faculty of Engineering, University of Porto  
Rua Dr. Roberto Frias, 4200-465, Porto, Portugal, (e-mail: idelfonso@fe.up.pt)*

---

**Abstract:** The Simulated Moving Bed (SMB) is a separation device whose use has been increasing, especially in separations that demand high purities like the chiral separation. Process Design is a topic often discussed in the literature and is usually limited to a sensitivity analysis. An optimal design of a SMB unit offers challenges due to its complexity on dynamics and numerical levels. Thus, there is a lack of a consistent methodology to optimize the SMB design. This work is focused on the SMB design which will be made using the Particles Swarm Optimization (PSO) method. For the first time, PSO will be used to choose the configuration, i.e., length of each section, of the True Moving Bed (the theoretical model of the SMB) unit for the case of the separation of the bi-naphthol enantiomers. The operating conditions, in terms of flowrates, will also be optimized. Globally, with the design strategy that was implemented, the system's productivity is at least 30% higher than previous results reported in the literature for the TMB without optimization of the device configuration. The SMB that was designed from this configuration enables to increase the separation productivity at least 20% in comparison with previous results.

**Keywords:** SMB, Process Design, Optimization, PSO, TMB

---

## 1. INTRODUCTION

The Simulated Moving Bed (SMB) is a separation device which operates according to the chromatographic principle. The SMB is constituted by a series of packed bed columns in which the inlet and outlet streams are synchronously switched in the direction of the fluid flow. The SMB has two inlets: the feed,  $F$ , and the eluent,  $E$ , and two outlets: the extract,  $X$ , and the raffinate,  $R$ . At the switching time,  $t^*$ , the inlets and outlets change their position cyclically. The synchronic switch of the SMB valves simulates a countercurrent contact between the solid and the liquid phases. In this way, it is possible to extend the chromatographic principle to large scale separations. In fact, the mass-transfer driving force is maximized, and a continuous injection is allowed (Rodrigues et al. 2015). The SMB has been gaining attention in the past years, especially for separations that require high purities (Pais et al. 1998, Zhang et al. 2002). Nowadays, several alternative versions of the original SMB have already been developed, such as Multifeed, Outlet Streams Swing (OSS) and Varicol (Rodrigues et al., 2015). The position of the inlet and outlet streams defines the four sections that exist in the SMB separation unit. Section I exists between the eluent and the extract streams, section II between the extract and the feed streams, section III between the feed and the raffinate streams and section IV between the raffinate and the eluent streams. The solid and the eluent are regenerated in sections I and IV, respectively, and the separation is accomplished in sections II and III (Rodrigues et al. 2015). The number of columns per section is called the *SMB* configuration which is decisive for the SMB performance. Frequently, the SMB is designed through sensitivity analysis, a trial and error and time-consuming process (Pais 1999, Dunnebie et al. 2000,

Azevedo and Rodrigues 2001, Lee et al. 2017, Lee and Seidel-Morgenstern 2018). To this day, there is not a systematic strategy to design SMB devices. Moreover, the configuration is normally defined independently of the operating conditions optimization. This prevents the separation process of using the SMB full capacity since the design is intrinsically related to the operating conditions and the performance of the SMB unit. The importance of analyzing the impact of column length on the SMB performance was already mentioned by Lee et al. (2017); however, it was not implemented yet. In this work, the SMB unit will be designed and optimized simultaneously for the first time. The optimization of complex systems such as True Moving Bed (TMB) and Simulated Moving Bed (SMB) has been done in the past years. Toumi et al. (2007) used algorithms based on the shooting method and Zang et al. (2002) studied the potential of genetic algorithms. Moreover, Matos et al. (2019) and Wu et al. (2006) used the Particles Swarm Optimization (PSO). Some organisms have a particular behavior called schooling that consists in staying together with their equals for defense and surviving purposes. This behavior of sharing information with others in order to move all the system has been studied and propelled the creation of algorithms. One of them is called Particles Swarm Optimization (PSO), which was developed by Eberhart and Kennedy (1995). In this method, a family of particles that keeps track of its coordinates is considered and used to optimize various systems. PSO has been gaining success when applied to the optimization of complicated systems due to its simple mathematics and reduced number of parameters (Eberhart and Kennedy, 1995; Eberhart and Shi, 2001). PSO has been used by Matos et al. (2019) to optimize a True Moving Bed (TMB) unit. However, the optimization only accounted for the operating conditions in terms of flowrates.

In this work, the PSO method will be used to fully design the SMB device. For the first time, the configuration of SMB will be taken into account. In the optimization process, which comprises the choice of the number of columns per section and the operating flowrates, the TMB model will be used. The TMB is the theoretical model behind the SMB concept. TMB considers that the solid actually moves in the opposite direction of the liquid. In this way, the TMB equations are much simpler to use in process simulation since the steady state can be directly obtained (Rodrigues et al., 2015). Since there is an equivalence between the TMB steady-state and the SMB cyclic steady-state, it is possible to use the TMB equations to simulate the SMB device. In this work, the SMB design will be done for the separation of the bi-naphthol enantiomers.

## 2. MATHEMATICAL MODELS

### 2.1 Particles Swarm Optimization (PSO) Algorithm

PSO is an algorithm that intends to reproduce the schooling behaviour. With this purpose, it considers a family of particles,  $n_p$ , in which each particle shares information with the others. Each particle has a number of dimensions,  $n_d$ , which is equal to the number of parameters to be optimized. At each iteration, the particles change their position (until the maximum number of iterations,  $n_{it}$ , is achieved) taking into account the position of the best positioned particle,  $x_{g_{best}}$ , and the best position of each particle,  $x_{p_{best}}$ . The system's dimension is equal to  $n_{it} \times n_p \times n_d$  (Matos, 2017). In the first iteration, each particle's position,  $x_p$ , (i.e., its value) and step,  $v$ , are given in (1) and (2), respectively (Eberhart and Kennedy, 1995),

$$x_p = x_{min} + R(x_{max} - x_{min}) \quad (1)$$

$$v = v_{max}(2R - 1) \quad (2)$$

where  $x_{min}$  and  $x_{max}$  are the minimum and maximum values for the optimization variables,  $R$  is a random number between 0 and 1 and  $v_{max}$  (Matos, 2017) is given by

$$v_{max} = \frac{x_{max} - x_{min}}{5} \quad (3)$$

From the second iteration to the maximum number of iterations,  $x_p$  and  $v$  are updated using (4) and (5), respectively (Matos et al. 2019).

$$x_p^{i+1} = x_p^i + v^{i+1} \quad (4)$$

$$v^{i+1} = wv^i + c_1R(x_{p_{best}}^i - x_p^i) \quad (5)$$

$$+ c_2R(x_{g_{best}}^i - x_p^i)$$

Where  $i$  is the iteration,  $x_{p_{best}}$  is the position of the best of each particle,  $x_{g_{best}}$  is the position of the best particle and  $w$ ,  $c_1$  and  $c_2$  are parameters.  $w$  represents the "resistance of the particle to its movement" (Matos et al. 2019) and is determined by

$$w = w_0 + (w_f - w_0) \frac{i}{n_{it}} \quad (6)$$

where  $w_0$  is the inertia weight at the beginning of the search and  $w_f$  is the inertia weight at the end of the search (Shi and Eberhart, 1998). In this work, the values for the initial and final inertia weights were 0.9 and 0.4, respectively (Ratnaweera et al, 2004; Eberhart and Shi, 2001).  $c_1$  and  $c_2$  were respectively calculated at each iteration by (7).

$$c_1 = \frac{(0.5 - 2.5)i}{n_{it}} + 2.5 \quad (7a)$$

$$c_2 = \frac{(2.5 - 0.5)i}{n_{it}} + 0.5 \quad (7b)$$

The algorithm is fully described elsewhere (Eberhart and, 1995) and is summarized in the following steps: Initialize the system ( $x_p$  and  $v$ ); Evaluate the objective function for each value of  $x_p$ ; Select  $x_{p_{best}}$  and  $x_{g_{best}}$ ; Update  $x_p$  and  $v$ ; Loop until the maximum number of iterations.

The adequation the referred PSO parameters for the bi-naphthol enantiomers system was previously shown by Matos (2017).

### 2.2 Simulated Moving Bed (SMB)

The SMB global balances are

$$u_e + u_{IV}' = u_I' \quad (8)$$

$$u_I' = u_{II}' + u_x$$

$$u_{feed} + u_{II}' = u_{III}'$$

$$u_{III}' = u_{IV}' + u_r$$

where  $u'$  are the fluid interstitial velocities of sections I, II, III and IV;  $u_{feed}$ ,  $u_r$ ,  $u_e$  and  $u_x$  are the feed, the raffinate, the eluent and the extract interstitial velocities, respectively. The mass balance to the fluid is

$$Dax_k' \frac{\partial^2 c_{ik}}{\partial z^2} - u_k' \frac{\partial c_{ik}}{\partial z} - \frac{1 - \varepsilon}{\varepsilon} k_L (q_{ik}^* - q_{ik}) = \frac{\partial c_{ik}}{\partial t} \quad (9)$$

Here,  $z$  represents the axial position and  $t$  represents the integration time,  $Dax_k'$  is the axial dispersion coefficient in column  $k$ ,  $c_{ik}$  is the concentration of compound  $i$  in column  $k$ , in the liquid phase,  $u_k'$  is the fluid interstitial velocity in column  $k$ ,  $\varepsilon$  is the bulk porosity,  $k_L$  is the mass transfer coefficient (considering LDF model),  $q_{ik}^*$  is the concentration of compound  $i$  in column  $k$ , in the solid phase in equilibrium with the liquid phase and  $q_{ik}$  is the concentration of compound  $i$  in column  $k$ , in the solid phase. The mass balance to the solid is

$$k_L (q_{ik}^* - q_{ik}) = \frac{dq_{ik}}{dt} \quad (10)$$

In the previous balances, the axial dispersion coefficient in column  $k$  is given by

$$Dax_k' = \frac{u_k' L_k'}{Pe} \quad (11)$$

where  $L_k'$  is the length of column  $k$  and  $Pe$  is the Peclet number.

The SMB initial conditions are expressed by

$$c_{ik} = q_{ik} = 0, \text{ at } t = 0 \quad (12)$$

The boundary conditions for column  $k$  are

$$c_{ik} - \frac{Dax_k' \partial c_{ik}}{u_k' \partial z} = c_{ik,0}, \text{ at } z = 0 \quad (13)$$

$$\frac{dc_{ij}}{dz} = 0, \text{ at } z = L_k'$$

$$\text{for the eluent node, } c_{i(k+1),0} = c_{ik} \frac{u_{IV}'}{u_I'}$$

$$\text{for the feed node, } c_{i(k+1),0} = \frac{u_{III}'}{u_{III}'} c_{ik} + \frac{u_{feed}}{u_{III}'} c_i^{feed} \quad (14)$$

$$\text{for the extract and raffinate nodes, } c_{i(k+1),0} = c_{ik}$$

### 2.3 True Moving Bed (TMB) model

As explained in the Introduction, the optimization process to design the SMB device, will be performed using the theoretical model, TMB. True Moving Bed (TMB) is a separation device in which the solid moves in the opposite direction in relation to the fluid. TMB has two inlet streams: the feed (A+B) and the eluent,  $e$ , and two outlet streams: the raffinate,  $r$ , (rich in the less-adsorbed compound, A) and the extract,  $x$ , (rich in the more-adsorbed compound, B). Both the solid and fluid are recycled. The TMB unit is divided into four sections (Rodrigues et al., 2015). In section I, compound B moves with the liquid. In section IV, A moves with the solid. In sections II and III A goes with the liquid and B with the solid. Fig. 1 represents schematically the TMB device, considering a feed with only two compounds, A and B. The circles represent the nodes.

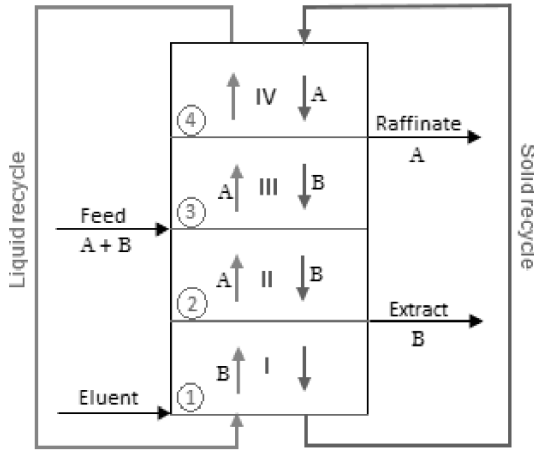


Fig. 1. Schematic representation of the TMB device. The TMB node balances are presented in (15):

$$\begin{aligned} u_e + u_{IV} &= u_I \\ u_I &= u_{II} + u_x \\ u_{feed} + u_{II} &= u_{III} \\ u_{III} &= u_{IV} + u_r \end{aligned} \quad (15)$$

where  $u_j$  are the interstitial fluid velocities in the section  $j$ ,  $u_{feed}$ ,  $u_r$ ,  $u_e$  and  $u_x$  are the feed, the raffinate, the eluent and the extract interstitial velocities, respectively. Note that the interstitial velocity is given by:

$$u = \frac{Q}{A\varepsilon} \quad (16)$$

where  $Q$  is the volumetric flowrate,  $A$  is the column section's area and  $\varepsilon$  is the porosity. The steady-state mass balance to the fluid is:

$$Dax_j \frac{d^2 c_{ij}}{dz^2} - u_j \frac{dc_{ij}}{dz} - \frac{1-\varepsilon}{\varepsilon} k_L (q_{ij}^* - q_{ij}) = 0 \quad (17)$$

Here,  $z$  represents the axial position,  $Dax_j$  is the axial dispersion in section  $j$ ,  $c_{ij}$  is the concentration of compound  $i$  in section  $j$  in the fluid phase,  $u_j$  is the fluids interstitial velocity in section  $j$ ,  $\varepsilon$  is the bulk porosity,  $k_L$  is the mass transfer coefficient (assuming LDF model),  $q_{ij}^*$  is the concentration of compound  $i$  in section  $j$  in the solid phase in equilibrium with the liquid phase and  $q_{ij}$  is the concentration of compound  $i$  in

section  $j$  in the solid phase. The steady-state mass balance to the solid is

$$u_s \frac{dq_{ij}}{dz} + k_L (q_{ij}^* - q_{ij}) = 0 \quad (18)$$

Where  $u_s$  is the solid velocity. In the previous balances, the axial dispersion coefficient in section  $j$  is given by

$$Dax_j = \frac{u_j L_j}{Pe} \quad (19)$$

where  $L_j$  is the length of section  $j$  and  $Pe$  is the Peclet number.

At section  $j$ , the boundary conditions for the liquid phase are given by

$$c_{ij} - \frac{Dax_j}{u_j} \frac{dc_{ij}}{dz} = c_{ij,0}, \text{ at } z=0 \quad (20a)$$

$$\frac{dc_{ij}}{dz} = 0, \text{ at } z = L_j$$

$$c_{iIV,L} = \frac{u_I}{u_{IV}} c_{iI,0}$$

$$c_{iI,L} = c_{iII,0} \quad (20b)$$

$$c_{iII,L} = \frac{u_{III}}{u_{II}} c_{iIII,0} - \frac{u_{feed}}{u_{II}} c_i^{feed}$$

$$c_{iIII,L} = c_{iIV,0}$$

The solid phase boundary conditions are expressed by

$$q_{iIV,L} = q_{iI,0} \quad (21)$$

$$q_{iI,L} = q_{iII,0}$$

$$q_{iII,L} = q_{iIII,0}$$

$$q_{iIII,L} = q_{iIV,0}$$

### 2.4 Equivalence between TMB and SMB

The equivalence between TMB and SMB in terms of velocities (by keeping the liquid velocity constant in relation to the solid velocity) or flowrates, respectively can be expressed by

$$u'_j = u_j + u_s \quad (22)$$

$$Q'_j = Q_j + \frac{1-\varepsilon}{\varepsilon} Q_s \quad (23)$$

where  $u_s$  is the solid velocity. Here,  $Q_s$  and the switching time,  $t^*$ , are respectively given by

$$Q_s = \frac{1-\varepsilon}{t^*} V_c' \quad (24)$$

$$t^* = \frac{L'}{u_s} \quad (25)$$

where,  $L'$  is the length of the SMB column and  $V_c'$  is the volume of the SMB column (Rodrigues et al., 2015, Pais 1999).

### 3. OPTIMIZATION STRATEGY

In this work, the optimization of the TMB operating conditions is done using the volumetric flow-rates as decision variables which are the eluent,  $Q_e$ , the extract,  $Q_x$ , the recycle,  $Q_{IV}$ , the feed,  $Q_{feed}$  and the solid,  $Q_s$ , volumetric flow-rates. To optimize the configuration, the section lengths,  $L_I$ ,  $L_{II}$  and  $L_{III}$  are added to the group of decision variables. The search dimension of the PSO algorithm is then equal to eight. The length of section IV,  $L_{IV}$ , is determined using the total bed length,  $L$ , according to

$$L_{IV} = L - L_I - L_{II} - L_{III} \quad (26)$$

The objective function used in this work is given in Equation 27 (Matos et al. 2019), which is a constrained function written in terms of the productivity and the eluent consumption.

$$Fobj = EC + \frac{1}{0.01 + Prod} + \omega \sum_{i=1}^2 f_i^2 \quad (27)$$

Subject to

$$[Prod; EC] \geq 0 \\ 1 \geq [Pr; Px] \geq 0$$

In which the productivity,  $Prod$ , is given by

$$Prod = Prod_x + Prod_r \quad (28)$$

$$Prod_x = \frac{Rec_x Q_{feed} C_B^{feed}}{(1 - \varepsilon) V_c N_c} \quad (29)$$

$$Prod_r = \frac{Rec_r Q_{feed} C_A^{feed}}{(1 - \varepsilon) V_c N_c} \quad (30)$$

where  $Rec_x$  and  $Rec_r$  are the extract and the raffinate recoveries, respectively,  $C_A^{feed}$  and  $C_B^{feed}$  are the feed concentration of A and B, respectively,  $\varepsilon$  is the bulk porosity,  $V_c$  is the TMB column volume and  $N_c$  is the number of columns (in the TMB case,  $N_c=1$ ). There are two end point constraints ( $[Prod; EC] \geq 0$ ,  $1 \geq [Pr; Px] \geq 0$ ) and a series of path constraints on the decision variables, which are evaluated along the optimization (Matos, 2017). The raffinate and extract recoveries are respectively determined by

$$Rec_r = \frac{Q_r C_A^r}{Q_{feed} C_A^{feed}} \quad (31)$$

$$Rec_x = \frac{Q_x C_B^x}{Q_{feed} C_B^{feed}} \quad (32)$$

where  $C_A^r$  and  $C_B^x$  are the mass concentrations of A and B in the raffinate and extract streams, respectively.

As a chiral separation is being performed, the eluent is also present in the feed; hence, the eluent consumption,  $EC$ , is calculated by

$$EC = \frac{Q_e + Q_{feed}}{Q_{feed} \sum_{j=1}^{nc} c^{feed}} \quad (33)$$

in which  $nc$  is the number of components (Nogueira et al. 2016).

In the objective function presented in Equation 27,  $\omega$  is the penalty coefficient and  $f_i$  is calculated by

$$f_i = P_i - P^{set} - |P_i - P^{set}| \quad (34)$$

in which  $P_i$  is the extract or the raffinate purity and  $P^{set}$  is the desired purity.

The raffinate and the extract purities are given by

$$P_r = \frac{C_A^r}{C_B^r + C_A^r} \quad (35)$$

$$P_x = \frac{C_B^x}{C_B^x + C_A^x} \quad (36)$$

### 3.1 Convergence Criteria

To perform the optimizations, the maximum number of iterations used was equal to 2000. The convergence criteria is then evaluated in terms of the number of iterations that was needed to attain convergence,  $n_{it}^*$ .

For each iteration and each dimension of  $x_p$ , the criterion  $\frac{|x_p - x_p^{it}|}{x_p} \times 100 \leq 1\%$  is applied. If the criterion  $\leq 1\%$  is verified for all dimensions,  $n_{it}^*=i$  and convergence is assumed to have been attained (Matos et al. 2019).

## 4. RESULTS AND DISCUSSION

To perform the PSO optimization was performed in MATLAB while TMB model reported in his work, was implemented in gPROMS and a communication between both software was done with gO:MATLAB, using a FPI (Foreign Process Interface) event. The simulations were run in a processor Intel® Core™ i5-2400 with a 3.10 GHz CPU. The RAM had an 8.00 GB capacity. The operating conditions are listed in Table 1.

**Table 1. Operating Conditions**

Total bed length, $L$ (dm)	8
Column diameter (dm)	0.26
Porosity, $\varepsilon$	0.4
Feed concentration (g/L)	2.9
Mass transfer coefficient, $k_L$ (min <sup>-1</sup> )	6
Peclet number, $Pe$	2000
Temperature, $T$ (K)	303.15

To simulate the separation of the bi-naphthol enantiomers, a Pirkle type stationary phase, the 3,5-dinitrobenzoyl phenylglycine covalently bonded to silica gel (3,5-DNBPG-Silica) was used. The particles had a diameter of 25-40  $\mu\text{m}$  and the eluent was a 72/28 heptane/isopropanol mixture. This system was studied by Pais (1999) who performed the experimental separation in a 12 column SMB (*Licosep* 12-26). The adsorption equilibrium isotherms were determined by the *Separex* group (Pais 1999):  $q_A^* = \frac{2.69c_A}{1+0.0336c_A+0.0466c_B} + \frac{0.10c_A}{1+c_A+3c_B}$  and  $q_B^* = \frac{3.73c_B}{1+0.0336c_A+0.0466c_B} + \frac{0.30c_B}{1+c_A+3c_B}$  in g/L.

### 4.1 PSO Optimization of TMB Model

The TMB will be optimized, considering the existence of all four sections, i.e., the length of each section is larger than  $0.01L$ . In this way, considering equal bounds for the sections that will be optimized, the maximum length for sections I, II and III is  $L/3$ . The optimization limits will then be between  $0.01L$  and  $L/3$ . From this optimization, a SMB device with four sections will be designed. The path constraints of the decision variables are presented in Table 2. For the optimization, ten runs of the PSO method were performed. To illustrate the results, the run with the highest productivity, the average and the standard deviation (STD) are shown in Table 3.

**Table 2. TMB decision variables constraints and optimization parameters.**

	<i>min</i>	<i>max</i>
$Q_E$ (mL/min)	0.01	200
$Q_X$ (mL/min)	0.01	200
$Q_{IV}$ (mL/min)	0.01	200
$Q_{feed}$ (mL/min)	0.01	200
$Q_s$ (mL/min)	0.01	200
$L_I$	0.01L	L/3
$L_{II}$	0.01L	L/3
$L_{III}$	0.01L	L/3
$n_{it}$	2000	
$n_d$	5	
$n_p$	50	
$\omega$	4000	
$w_0$	0.9	
$w_f$	0.4	
$c1_0$	0.5	
$c1_f$	2.5	
$c2_0$	2.5	
$c2_f$	0.5	
$p^{set}$	0.97	

**Table 3. TMB optimization results, TMB-L, (flow-rates in mL/min, productivity in g/L<sub>ads</sub>/day, eluent consumption in dL/g and section's length in dm).**

	TMB-L (best run)	TMB-L (average)	TMB-L (STD)	Matos et al. 2019	Wu et al. 2006
$Q_E$	80.8	78.4	2.3	27.4	22.1
$Q_X$	49.5	50.6	2.2	24.1	19.6
$Q_{IV}$	13.6	16.6	3.9	27.6	21.5
$Q_{feed}$	9.9	9.8	0.06	7	4.4
$Q_s$	17.5	17.3	0.35	12.1	9.0
$L_I$	1.8	1.7	0.18	-	-
$L_{II}$	2.8	2.8	0	-	-
$L_{III}$	2.8	2.8	0	-	-
$P_r$	0.97	0.97	0	0.97	0.99
$P_x$	0.97	0.97	0	0.97	0.98
<i>Prod</i>	299.5	297.3	2.1	212.3	144.0
<i>EC</i>	93.5	90.8	2.7	84.9	-
$n_{it}^*$	1801	1849	69	1888	-

Comparing Table 3 results with a representative run of the optimization(ii) results previously reported by Matos et al. (2019) for the same system it is visible that adding the sections length as an optimization variable leads to a better operating point since the productivity significantly increased (almost 30%). The eluent consumption slightly increased (5%) and the purities constraints were respected. The productivity of this work is about 50% higher than the results reported by Wu et al. (2006) for the optimization of the same system. As expected, this result shows that the length of the TMB sections plays a major role on the performance of the device, confirming that the design should be done in parallel with the optimization of the operating conditions (Matos 2017).

#### 4.2 SMB Design

As shown in Table 3, the TMB configuration, i.e., the length of each section, in dm, obtained for TMB-L is 1.8-2.8-2.8-0.6. Normalizing in order to obtain an integer number of columns per section, the SMB configuration is 3-5-5-1. The SMB simulation was then performed, considering the configuration 3-5-5-1 (total number of columns equal to fourteen). The operating conditions were obtained from equations in section 2.4:  $Q_E=80.8$  mL/min,  $Q_X=49.5$  mL/min,  $Q_{IV}=25.3$  mL/min,  $Q_{feed}=9.9$  mL/min and the switching time,  $t^*=2.18$  min. The productivity, the raffinate and the extract purities were, respectively, calculated by

$$Prod = \frac{Q_R \int_t^{t+N_c t^*} c_A^R dt}{(1-\varepsilon)V_c N_c t^*} + \frac{Q_X \int_t^{t+N_c t^*} c_B^X dt}{(1-\varepsilon)V_c N_c t^*} \quad (37)$$

$$P_R = \frac{\int_t^{t+N_c t^*} c_A^R dt}{\int_t^{t+N_c t^*} c_A^R dt + \int_t^{t+N_c t^*} c_B^R dt} \quad (38)$$

$$P_X = \frac{\int_t^{t+N_c t^*} c_B^X dt}{\int_t^{t+N_c t^*} c_A^X dt + \int_t^{t+N_c t^*} c_B^X dt} \quad (39)$$

This simulation results and the comparison with the TMB are shown in Table 4.

**Table 4. Results and comparison with TMB**

	$P_R$	$P_X$	<i>Prod</i> (g/L <sub>ads</sub> /day)	<i>EC</i> (dL/g)
SMB14	0.97	0.96	288.0	93.4
TMB-L	0.97	0.97	299.5	93.5

Comparing with the TMB-L results, Table 4 shows that the intended extract purity is not attained. The productivity decreased 1% and the eluent consumption is nearly the same. Despite these differences the result is quite good, considering that a different model is being used.

The internal concentration profiles are represented in Fig. 2.

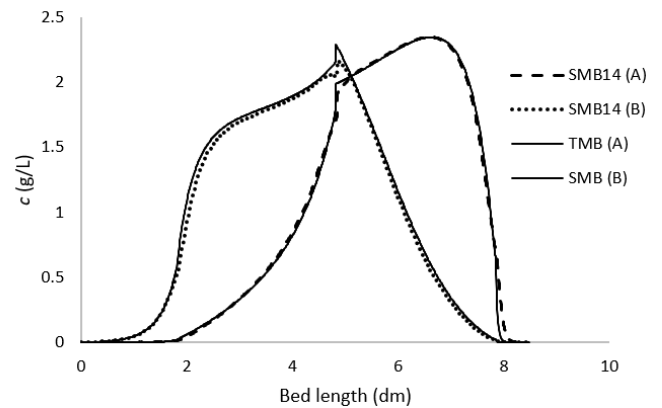


Fig. 2. Steady state internal concentration profiles of the less (A) and the more (B) retained species for TMB and SMB14 at half of the switching time.

As expected, the TMB and SMB concentration profiles are almost overlapped. In fact, the extract purity in the SMB simulation did not achieve the desired 97%, which is explained by the differences in the profiles of Fig. 2.

In order to achieve the desired purity for both extract and raffinate, two different approaches can be used: adjusting the

operating conditions or increasing the number of columns per section from the original configuration 3-5-5-1.

Concerning the operating conditions adjustment, purities of 97% can be achieved if the switching time is increased 0.2% as suggested by Nogueira et al. (2016) who studied the process dynamics of the bi-naphthol enantiomers' system. Table 5 shows the comparison of this approach, SMB14-t, with the previous results SMB14 and with the best result reported by Matos et al. (2019).

**Table 5. SMB-t results and comparison with SMB**

	$P_R$	$P_X$	$Prod (g/L_{ads} \text{ day})$	$EC(dL/g)$
SMB14-t	0.97	0.97	287.9	93.4
SMB14	0.97	0.96	288.0	93.4
SMB12(Matos et al. 2019)	0.97	0.96	202.5	84.7

Table 5 shows that the change in the switching time enables to achieve the desired purities without compromising the productivity, which only decreased 0.03 %. The eluent consumption was not affected. Comparing this result with Matos et al. (2019), it is visible that performing the SMB optimization including the design enables to increase the productivity 30%. As expected, the SMB configuration plays a major role on the performance of the device.

## 5. CONCLUSIONS

The TMB configuration exerts a massive influence in the separation performance of the device. A much higher productivity was obtained for the bi-naphthol system, comparing to the results previously published in the open literature: 30% higher than Matos et al. 2019 and 50% higher than Wu et al. 2006. The TMB results were used to define the SMB configuration (i.e., number of columns per section). It was shown that, defining the SMB design from the optimization enables to increase the productivity of the SMB separation. Several configurations were presented in which the productivity increased at least 20% in relation to the result reported by Matos et al. (2019).

## REFERENCES

- Azevedo, D.C.S., Rodrigues, A.E. Rodrigues. (2001). Design methodology and operation of a simulated moving bed reactor for the inversion of sucrose and glucose-fructose separation. *Chem. Eng. J.*, 82, 95-107.
- Dunnebier, G., Fricke, J., Klatt, K. (2000). Optimal Design and Operation of Simulated Moving Bed Chromatographic Reactors. *Ind. Chem. Res.*, 39, 2290-2304.
- Eberhart, R.C, Kennedy, J. (1995). A New Optimizer Using Particle Swarm Theory. *Proceedings of the Sixth International Symposium on Micro Machine and Human Science*.
- Eberhart, R.C., Shi, Y. (2001). Particle Swarm Optimization: Developments, Applications and Resources. *Proceedings of the 2001 Congress on Evolutionary Computation*, 1, 81-86.
- Lee, C., Choi, J., Park, C., Wang, N.L., Mun, S. (2017). Standing wave design and optimization of a simulated moving bed chromatography for separation of xylobiose and xylose under the constraints on product concentration and pressure drop. *J. Chromatogr. A*, 1527, 80-90.
- Lee, J.W., Seidel-Morgenstern, A. (2018). Model Predictive Control of Simulated Moving Bed Chromatography for Binary and Pseudo-binary Separations: Simulation Study. *IFAC*, 51-18, 530-535.
- Matos, J. (2017). *Particles Swarm Optimization for Chiral Separation by True Moving Bed Chromatography*. Master's Thesis. Faculdade de Engenharia da Universidade do Porto.
- Matos, J., Faria, R.P.V., Nogueira, I.B.R., Loureiro, J.M., Ribeiro, A.M. (2019). Optimization strategies for chiral separation by true moving bed chromatography using Particles Swarm Optimization (PSO) and new Parallel PSO variant. *Computers and Chemical Engineering*, 123, 344-356.
- Nogueira, I.B.R., Ribeiro, A.M., Rodrigues, A.E., Loureiro J.M. (2016). Dynamics of a True Moving Bed separation process: Effect of operating variables on performance indicators using orthogonalization method. *Computers and Chemical Engineering*, 86, 5-17.
- Pais, L.S., Loureiro, J. M., Rodrigues, A.E. (1998). Modeling Strategies for Enantiomers Separation by SMB Chromatography. *AIChE Journal*, 44 (3), 561-69.
- Pais, L.S. (1999). *Chiral Separation by Simulated Moving Bed Chromatography*. PhD Thesis. Faculdade de Engenharia da Universidade do Porto.
- Ratnaweera, A., Halgamuge, S.K., Watson, H.C. (2004). Self-Organizing Hierarchical Particle Swarm Optimizer with Time-Varying Acceleration Coefficients. *IEEE Transactions on Evolutionary Computation*, 8(3),240-55.
- Rodrigues, A.E., Pereira, C., Minceva, M. Pais, L.S., Ribeiro, A. Ribeiro, A.M, Silva, M., Graça N., Santos, J.C. (2015). *Simulated Moving Bed Technology*. Edited by Fiona Gerghty. Joe Hayton.
- Toumi, A., Engell, S., Diehl, M. Bock, H.G., Schl, J. (2007). Efficient Optimization of Simulated Moving Bed Processes. *Chemical Engineering and Processing: Process Intensification*, 46, 1067-84.
- Wu X., Jin, X., Xu, Z., Wang, S. (2006). Application of Particle Swarm Optimization in Process of Non-Linear Simulated Moving Bed Chromatographic Fractionation. *Control and Instruments in Chemical Industry*, 33, 5-9.
- Zhang, Z., Hidajat, K., Ray, A.K., Morbidelli, M. (2002). Multiobjective Optimization of SMB and Varicol Process for Chiral Separation. *AIChE Journal*, 48 (12), 2800-2816.

## ACKNOWLEDGMENTS

This work was financially supported by: EDUFI Fellowships program, Base Funding - UIDB/50020/2020 of the Associate Laboratory LSRE-LCM - funded by national funds through FCT/MCTES (PIDDAC); FCT – Fundação para a Ciência e Tecnologia under CEEC Institucional program and scholarship SFRH/BD/137094/2018.